Disorder in Zeolite SSZ-31 Described on the Basis of One-Dimensional Building Units

Henk van Koningsveld†

Laboratory of Applied Organic and Catalytic Chemistry, DelftChemTech, Delft University of Technology, Julianalaan 136, 2628 BL Delft, The Netherlands

Raul F. Lobo*

Center for Catalytic Science and Technology, Department of Chemical Engineering, University of Delaware, Newark, Delaware 19716

Received: October 30, 2002; In Final Form: July 18, 2003

A new description of the disorder in SSZ-31 is given on the basis of one-dimensional units consisting of tubular pores. The pores are formed of rolled-up honeycomb-like sheets of fused T6-rings (T = tetrahedral) and the pore aperture contains 12 T atoms. The 1-D units are arranged into different types of layers depending on whether the shift between adjacent pores in the layer is zero or one-half of the repeat distance along the pore. These layers of pores can be used to build three-dimensional framework structures. This approach has led to two new findings: first, two new polytypes have been found—in addition to eight polytypes previously described—and second, it is shown that it is possible to have intergrowths between all 10 polytypes and not only among selected groups of them—as previously thought. Simulation of the X-ray diffraction patterns of disordered structures indicate that SSZ-31 is even a more disordered structure than previously reported. The disorder does not block the pores and the local pore topology is the same in all (disordered) models. Differences in catalytic behavior of different samples of SSZ-31 are probably due to differences in synthesis conditions (Si/Al ratio), distribution of the Al over the framework positions, and size and morphology of the crystals.

1. Introduction

SSZ-31 is a family of high-silica zeolite materials containing a one-dimensional pore system with a T12 ring pore aperture (T = tetrahedral atom).[1] Several synthetic studies of this zeolite family have been reported using the so-called dry-gel method,[2] by transformation of other zeolites,[3,4] using the fluoride method,[5]or by direct synthesis.[6] The aluminum-containing forms of SSZ-31 are shape-selective alkylation catalysts[7] and have been used, for example, for the alkylation of biphenyl.[8,9]

The SSZ-31 materials are highly faulted and can be thought to be intergrowths of four different but related polytypes (polytypes **A**−**D**). Four additional polytypes (**E**−**H**) have been described, but interconnection between these four (**E**−**H**) and the previous four (**A**−**D**) leads to highly strained subunits that are unlikely to be found in actual materials.[1] Better understanding of zeolite structure is a crucial prerequisite to understanding catalytic properties. This is even more so in disordered materials where disorder can affect the diffusion of molecules in the channels.

This report delves more deeply into the disorder of SSZ-31. The polytypes **A**−**D** can be constructed from two different types of T28 units. These T28 units form chains along ***a*** and the chains are connected into 5^46^1 layers parallel to (001) as shown in Figure 1. In the description of Lobo et al.,[1] the polytypes are formed by connecting 5^46^1 layers via double crankshaft chains. In the monoclinic polytypes **A** and **C**, shown in Figure 1, the 5^46^1 layers are related by lateral translations along ***c*** (and ***b***). The orthorhombic polytypes **B** and **D** (not shown) are obtained when, in addition to the lateral shift(s), neighboring 5^46^1 layers (***ab*** layers) are rotated with respect to each other over 180° about the plane normal before connecting them by double crankshaft chains. All pores are formed solely of cylindrical nets of (fused) T6-rings.

Transmission electron microscopy (TEM) images reveal[1] the presence of stacking faults along the ***ab***-plane normal ***n*** caused by displacements of ***ab*** layers over approximately one-third of the lateral repeat distance ***a***. In agreement with these displacements, the ED pattern of the *h*0*l* projection[1] shows rows of sharp spots for $h = 3n$ and twinspots/diffuse streaks for $h \neq 3n$. No diffuse scattering is observed in the *h*0*l* pattern for $l \neq 3n$. This means that stacking faults, caused by displacements of layers parallel to (100) over one-third of the lateral repeat distance ***c***, are unlikely. The ED pattern of the *hk*0 projection[1] has alternating rows of sharp and streaked spots, suggesting stacking faults of layers parallel to (100) involving translations of $^1/_2\boldsymbol{b}$.

In a recent report,[10] a new way of looking at the disorder in zeolite ZSM-48 was described. This approach starts from a one-dimensional basic building unit: the T10-ring pores. The 1-D pores are formed of rolled-up honeycomb-like sheets of fused T6-rings and can be arranged into layers of pores. These layers of T10-ring pores can be stacked following certain rules to form a three-dimensional tetrahedral framework. It has been found here that the same approach can be used to describe the structure of zeolites SSZ-31 leading to two important findings:

1. There are two new additional polytypes of SSZ-31 (polytypes **I** and **J**).

* Corresponding author. Fax: (302) 831-2085. E-mail: lobo@che.Udel.edu.
† Fax: 31-15-278-1413. E-mail: h.vankoningsveld@tnw.tudelft.nl.

10.1021/jp027341e CCC: $25.00
Published on Web 09/16/2003

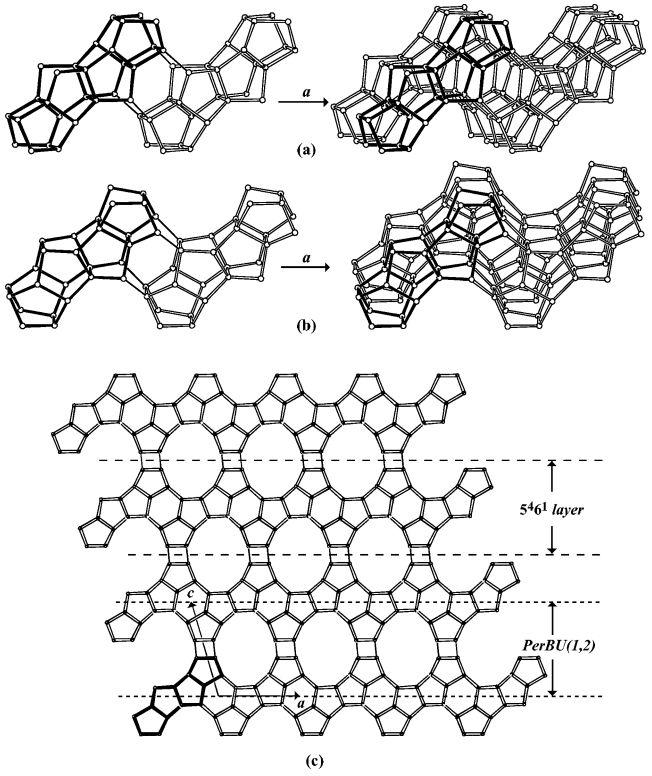

Figure 1. (a) and (b) Left: T-28 units (one in bold), related by pure translations along ***a***, are connected into chains parallel to ***a*** by T6-rings. The T28-units in (a) and (b) have a different topology and form polytypes (**A** and **B**) and (**C** and **D**), respectively. Right: Chains, related by pure translations along ***b***, are connected into 5^46^1 layers (***ab*** layers). (c) Parallel projection of the unit cell content in the monoclinic polytypes **A** and **C**. Neighboring ***ab*** layers, related by pure translations along ***c*** (in polytype **A**) or by pure translations along ***c*** accompanied by a shift of $^1/_2$***b*** (in polytype **C**), are connected by double crankshaft chains of the narsarsukite type. Periodic Building Units (PerBUs, see Section 2) are indicated.

2. A new way of interconnecting polytypes **A**−**D** with polytypes **E**−**H** has been found. This new interconnection avoids the formation of the strained structural subunits described above (see ref 1).

In this manuscript this new way of describing the structure of SSZ-31 materials is explained and the effect of intergrowths between polytypes **A**−**D**, **E**−**H**, and **I**−**J** on the simulated powder X-ray diffraction patterns (XRD) and electron diffraction patterns is investigated. The simulations indicate that SSZ-31 materials are better described as intergrowths of the (now) 10 polytypes rather than only 4 polytypes as was suggested previously. The inclusion of domains of polytypes **E**−**H** in the fault model is crucial. The present description accounts for the TEM and ED results reported by Lobo et al.[1]

2. Description of Zeolite SSZ-31 as an Array of Tubular Pores

In this section it is shown that SSZ-31 can be conceived as an array of T12-ring pores. To facilitate calculations, two types of layers (built from connecting pores) are used.

i. Periodic Building Units. The SSZ-31 polytypes can be built using the crankshaft chain (bold in Figure 2a; left). The repeat unit of the chain consists of 4 T-atoms and the repeat distance in the chain is ∼8.4 Å. Six crankshaft chains are connected to form a pore with a T12-ring window. The pore wall consists entirely of fused T6-rings. The repeat unit of the tubular pore is a T6-ring band of 24 T-atoms (bold in Figure 2a; right).

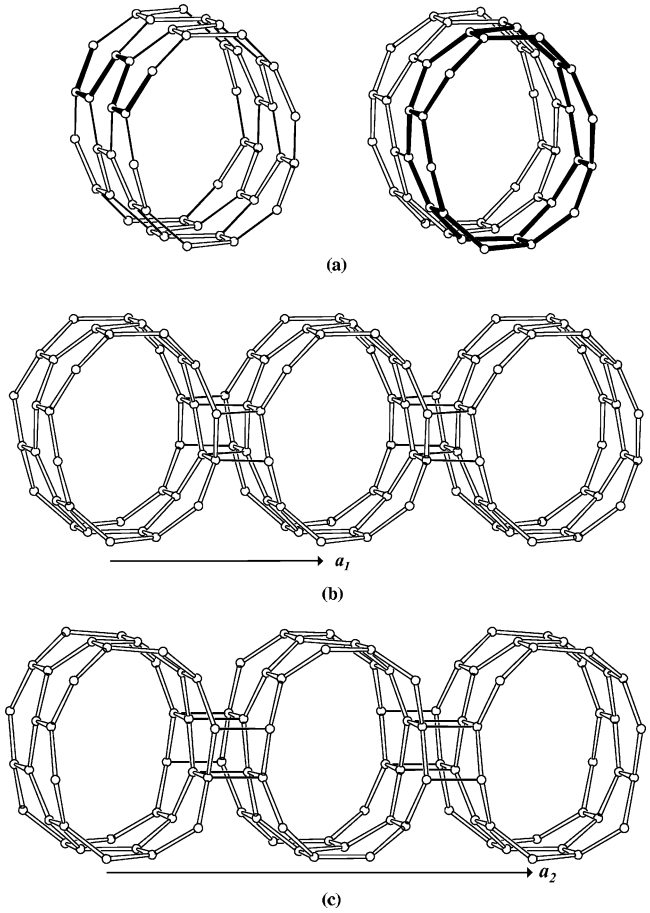

Figure 2. Tubular pores and PerBU(1,2) in SSZ-31. In (b) and (c) only $1^1/_2$ of the repeat unit along the pore axis of the PerBUs is drawn for clarity. (a) Pore with T12-ring window constructed from six crankshaft chains (left) and from T6-ring bands each consisting of 24 T atoms (right). (b) Tubular pores, related by pure translations along $\boldsymbol{a_1}$, are connected into PerBU1 through double crankshaft chains of the narsarsukite type. (c) Tubular pores, related by a translation of $^1/_2\boldsymbol{a_2}$ along $\boldsymbol{a_2}$ and a shift of $^1/_2$***b*** along the pore axis, are connected into PerBU2 through double crankshaft chains of the feldspar type.

The pores can be considered as being formed of rolled up honeycomb-like sheets of fused T6-rings. Neighboring pores can be connected into layers, hereafter called Periodic Building Units (PerBUs), with or without shifting them with respect to each other along the pore direction ***b***. The nonzero shift is equal to half the repeat distance along ***b***, which is equal to half the repeat distance in the crankshaft chain ($\sim^1/_2 \times$ 8.4 Å). The nonzero shift of $^1/_2$***b*** along the pore axis ***b*** is equivalent to a rotation of 30° (= 360/12) of the pore about the pore axis. In this paper we will use the "shift" description.

In PerBU1 (Figure 2b), neighboring pores, related by a pure translation along $\boldsymbol{a_1}$ and a zero shift along the pore axis ***b***, are connected through double crankshaft chains of the narsarsukite-type running parallel to ***b***. In PerBU2 (Figure 2b), neighboring pores, related by a translation of $^1/_2$ $\boldsymbol{a_2}$ along $\boldsymbol{a_2}$ and a shift of $^1/_2$***b***, are connected through double crankshaft chains of the feldspar type. Figure 1 shows that the PerBUs, used in the present description of the polytypes, are parallel to (001). The PerBUs are shifted with respect to the layers used in ref 1 by $^1/_2$***c***.

TABLE 1: Simplest Ordered Polytypes of SSZ-31 Described in the Standard Setting of the Space Group

Name	Descriptor[a]	Connection Modes[b]	Space Group	a	b (Å)	c	β (°)
		PerBU1					
A	○ ○ ○ ○ ○ ○ ○ ○ ○	($-^1/_6$, 0; $-^1/_6$, 0; $-^1/_6$, 0; …)	P2/m	12.35	8.4	14.97	106.0
B	○ ○ ○ ○ ○ ○ ○ ○ ○	($-^1/_6$, 0; $+^1/_6$, 0; $-^1/_6$, 0; …)	Pmna	8.4	12.35	28.78	-
C	○ ○ ○ ● ● ● ○ ○ ○	($-^1/_6$, $^1/_2$; $-^1/_6$, $^1/_2$; $-^1/_6$, $^1/_2$; …)	C2/m	29.94	8.4	12.35	106.0
D	○ ○ ○ ● ● ● ○ ○ ○	($-^1/_6$, $^1/_2$; $+^1/_6$, $^1/_2$; $-^1/_6$, $^1/_2$; …)	Pbcm	12.35	28.78	8.4	-
		PerBU2					
E	○ ● ○ ○ ● ○ ○ ● ○	($-^1/_6$, 0; $-^1/_6$, 0; $-^1/_6$, 0; …)	C2/m	24.70	8.4	14.97	106.0
F	○ ● ○ ○ ● ○ ○ ● ○	($-^1/_6$, 0; $+^1/_6$, 0; $-^1/_6$, 0; …)	Cmca	8.4	24.70	28.78	-
G	○ ● ○ ● ○ ● ○ ● ○	($-^1/_6$, $^1/_2$; $-^1/_6$, $^1/_2$; $-^1/_6$, $^1/_2$; …)	C2/m	24.70	8.4	16.58	119.8
H	○ ● ○ ● ○ ● ○ ● ○	($-^1/_6$, $^1/_2$; $+^1/_6$, $^1/_2$; $-^1/_6$, $^1/_2$; …)	Cmca	8.4	24.70	28.78	-
		PerBU1 and PerBU2					
I	○ ○ ○ ○ ● ○ ○ ○ ○	($-^1/_6$, 0; $-^1/_6$, 0; $-^1/_6$, 0; …)	P2/m	29.94	8.4	24.70	106.0
J	○ ○ ○ ○ ● ○ ○ ○ ○	($-^1/_6$, 0; $+^1/_6$, 0; $-^1/_6$, 0; …)	Pma2	8.4	28.78	24.70	-

[a] Empty (○) and filled (●) circles depict pores that are related by translations of $^1/_2 \times 8.4$ Å along the pore direction. [b] The connection modes refer to the displacement along ***a*** and ***b*** between consecutive PerBUs (***a*** = 24.7 Å and ***b*** = 8.4 Å).

ii. Connectivity of the Periodic Building Units. The stacking of PerBUs along their plane normal ***n***, requires a lateral shift of the PerBUs along ***a*** (and ***b***). The magnitude of ***n*** is equal to the "thickness" of each PerBU: $|\boldsymbol{n}| = 14.97 \cdot \sin(106°) = 14.39$ Å for polytype **A** (see Table 1). This description is used in the calculations with DIFFaX.[11]

It is convenient to describe the stacking sequence of the PerBUs along ***n*** using the same coordinate system in both PerBUs. Therefore the unit cell length along the ***a*** axis is taken equal to $2 \times |\boldsymbol{a_1}|$ in PerBU1 and equal to $|\boldsymbol{a_2}|$ in PerBU2. For both PerBUs, the lateral shifts along ***a*** are then given as $\pm^1/_6\,\boldsymbol{a}$. Direct neighboring PerBUs can be stacked along ***n*** in four different ways according to the lateral shift of the top layer along ***a*** and ***b***:

(a) $-^1/_6\,\boldsymbol{a}$ and zero; denoted as ($-^1/_6$, 0),
(b) $^1/_6\,\boldsymbol{a}$ and zero; denoted as ($^1/_6$, 0),
(c) $-^1/_6\,\boldsymbol{a}$ and $^1/_2\,\boldsymbol{b}$; denoted as ($-^1/_6$, $^1/_2$),
(d) $^1/_6\,\boldsymbol{a}$ and $^1/_2\boldsymbol{b}$; denoted as ($^1/_6$,$^1/_2$).

The connection modes (a) and (c) between PerBU1s, and for the connection modes (b) and (d) between PerBU2s are illustrated in Figure 3. Adjacent PerBUs are connected through T4-rings or crankshaft chains, depending on whether the shift along ***b*** between direct neighboring pores is zero or $^1/_2\boldsymbol{b}$, respectively. The gaps between the T6-ring pores are filled by T−T dimer units connected through additional T4-rings and crankshaft chains. The positions of the bridging oxygen atoms between the two PerBUs are hardly influenced by whether the PerBUs are connected through T4-rings or through crankshaft chains. The changes in positions of the bridging atoms caused by the lateral shift between adjacent pores of $^1/_2\boldsymbol{b}$ is small. If these small changes are neglected, the positions of the bridging oxygen atoms before and after a lateral shift of $\pm^1/_6\boldsymbol{a}$ has been applied are related by a rotation of 180° about the plane normal. This is important because this allows the formation of stacking faults between layers with only minor energetic penalties, whether the stacking faults are caused by displacements of $^1/_2\boldsymbol{b}$ or $\pm^1/_6\boldsymbol{a}$.

Once the distribution of the lateral shifts between the PerBUs along their plane normal is known, the three-dimensional framework is defined. For example, polytype **A** is obtained when neighboring PerBU1s are recurrently stacked along their plane normal with lateral shifts of $-^1/_6\,\boldsymbol{a}$ and no shift along ***b*** (connection mode (a)). Polytype **G** is obtained when neighboring PerBU2s are recurrently stacked along their plane normal with lateral shifts of $-^1/_6\,\boldsymbol{a}$ and $^1/_2\boldsymbol{b}$ (connection mode (c)).

3. Simplest Polytypes in the SSZ-31 Family of Frameworks

The systematic stacking of PerBU1 and PerBU2 using the connection modes described above gives rise to a series of 10 simplest ordered polytypes (Table 1 and Figure 4). For example,

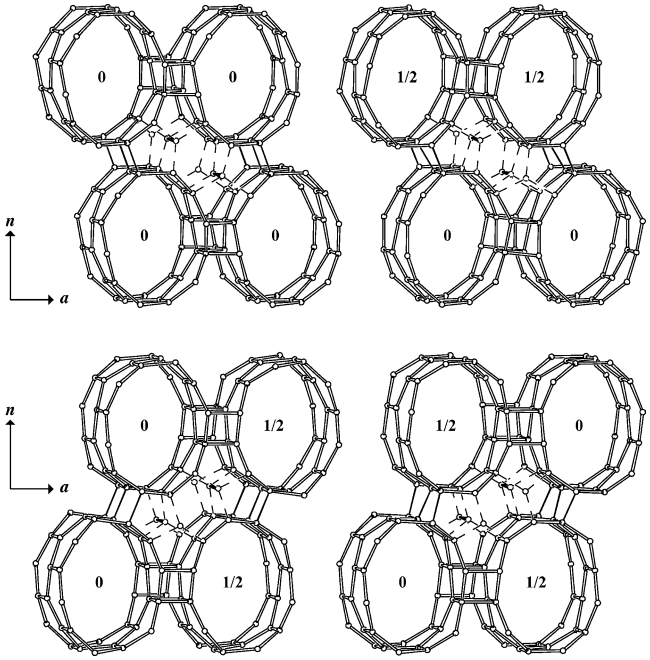

Figure 3. Illustration of connection modes in the SSZ-31 family of zeolites. Connecting T−T modes between PerBUs are drawn as single lines and the connections to the space filling T−T dimers (in heavy bold) between the pores are striped. Bridging oxygen atoms (not drawn) are about midway between T−T connections. The number in the pore gives the fractional shift of the pore along the pore axis ***b***. Top left and right: connection modes (a) and (c) between PerBU1s. Bottom left and right: connection modes (b) and (d) between PerBU2s.

polytype **A** is generated stacking PerBU1 using the ($-^1/_6$, 0) connection mode; polytype **F** is generated stacking PerBU2 using the ($-^1/_6$, 0) and the ($^1/_6$, 0) connection modes sequentially; polytype **I** is generated alternating PerBU1 and PerBU2 through a ($-^1/_6$, 0) connection mode. Polytypes **A**−**D** are generated from PerBU1, **E**−**H** from PerBU2, and **I** and **J** from alternating PerBU1 and PerBU2.

To the best of our knowledge, none of the polytypes has been observed yet as pure phase material. Table 1 provides the symmetry (using the standard setting) and unit cell dimensions of these polytypes, and Figure 4 illustrates the structure of four of them (a complete version of Figure 4 will be presented in the "Catalog of Disorder in Zeolite Frameworks"[12]). The atomic positions have been optimized using the Cerius[2] (ref 13) implementation of DLS-76, and in all cases reasonable agreement values are obtained. Intergrowth of the polytypes is achieved without changing the T6-ring pore topology. The gaps between the T6-ring pores are filled by T−T dimer units connected through additional T4-rings and crankshaft chains. Intergrowth introduces differences in the connection of dimers in the "empty" spaces.

The XRD patterns of these polytypes have been simulated (Figure 5). On the basis of the appearance of these patterns, the polytypes can be classified into two groups: the monoclinic polytypes (**A**, **C**, **E**, **G**, and **I**) and the orthorhombic polytypes (**B**, **D**, **F**, **H,** and **J**). An experimental XRD of a SSZ-31 material resembles more closely the ones with monoclinic symmetry (see Figure 5). Despite the similarities, however, none of these patterns agrees well with the experimental pattern; in order to obtain good agreement between experiment and simulation, the effect of the faulting, particle size, and morphology needs to be included, as will be shown below.

4. Simulation of XRD Patterns of Faulted Structures

There is a close analogy between the formation of faulted structures in SSZ-31 and ZSM-48. Consequently, the formation of disordered structures of SSZ-31 will be described along the same lines that disorder and stacking faults were described for ZSM-48.[10] The diffraction patterns of the faulted structures are simulated using the program DIFFaX.[11] For the purpose of these simulations, three distinct fault probabilities will be defined:

i. Alpha (α) determines the fraction of PerBU1 that forms a particular intergrowth. That is, α is the probability that after a particular layer *i*, the next layer is PerBU1. ($1 - \alpha$) then determines the fraction of PerBU2 that forms the structure.

ii. Beta (β) defines the probability of changing the fault direction. This means that if a series of PerBUs have been stacked following the ($-^1/_6$, 0) or the ($-^1/_6$, $^1/_2$) connection modes, the next layer will be stacked in the other direction (i.e., the $^1/_6$, 0 or the $^1/_6$, $^1/_2$) with a probability equal to β. Thus for $\beta = 0$, one of the monoclinic polytypes (**A**, **C**, **E**, **G,** or **I**) will be obtained; for $\beta = 1$, one of the orthorhombic polytypes (**B**, **D**, **F**, **H**, or **J**) will be obtained (see Table 2).

iii. Gamma (γ) defines the probability that the next layer will be stacked following the ($\pm^1/_6$, $^1/_2$) connection mode. This implies a translation of $^1/_2$ ***b*** along the pore direction. Thus, if $\gamma = 0$, polytypes **A**, **B**, **E**, **F**, **I,** or **J** are obtained; if $\gamma = 1$, polytypes **C**, **D**, **G**, **H**, **I** ,or **J** are obtained (see Table 2).

The parameters α, β, and γ are independent of each other and have values in the range 0−1. The first eight simplest polytypes can be simulated using specific values of α, β, and γ (see Table 2 for details). Simulations of XRD patterns of intergrowths of different polytypes for intermediate values of α, β, and γ are carried out using DIFFaX.[11] These simulations reveal that, to match the width and relative intensity of the first three peaks of the experimental diffraction pattern, the value of β must be in the range 0.20 to 0.25. This is in full agreement with earlier findings.[1] Therefore, in all subsequent calculations the value of β has been kept fixed at $\beta = 0.25$.

Figure 6 compares the XRD patterns of five intergrowths obtained for a constant value of $\beta = 0.25$ and values of α and γ either 0 or 1. There are many similarities between the patterns. First, the relative intensity and peak width of the first three peaks of these patterns are identical. Second, the peaks at 11°, the two peaks at ∼15°, the peaks at 21°, 22.5°, 25°, and 31° are present in all calculated patterns with nearly the same intensity. Finally, when compared to the patterns of the pure polytypes in Figure 5, many peaks have almost disappeared due to stacking faults. However, there still remain many peaks in the calculated patterns that are absent in the experimental one. This is an indication that, on one hand, there is more disorder in actual samples of SSZ-31 than is accounted for in these simple intergrowths. On the other hand, broadening of the XRD pattern due the particle size cannot be neglected as will be discussed below.

An extensive number of simulations have been carried out for a variety of values of α and γ (keeping $\beta = 0.25$). The main observation from these calculations is that the XRD pattern does not show large changes for values of α and γ in the range of 0.25−0.75. Given that the XRD patterns of samples of SSZ-31 suffer from anisotropic broadening due to the crystal size and morphology, it is considered that at this point it is not possible to determine precise values of α and γ for the sample of SSZ-31 investigated. It does seem, however, that those patterns that incorporate both PerBU1 and PerBU2 as the building units ($0 < \alpha < 1$) are in better agreement with the measurement

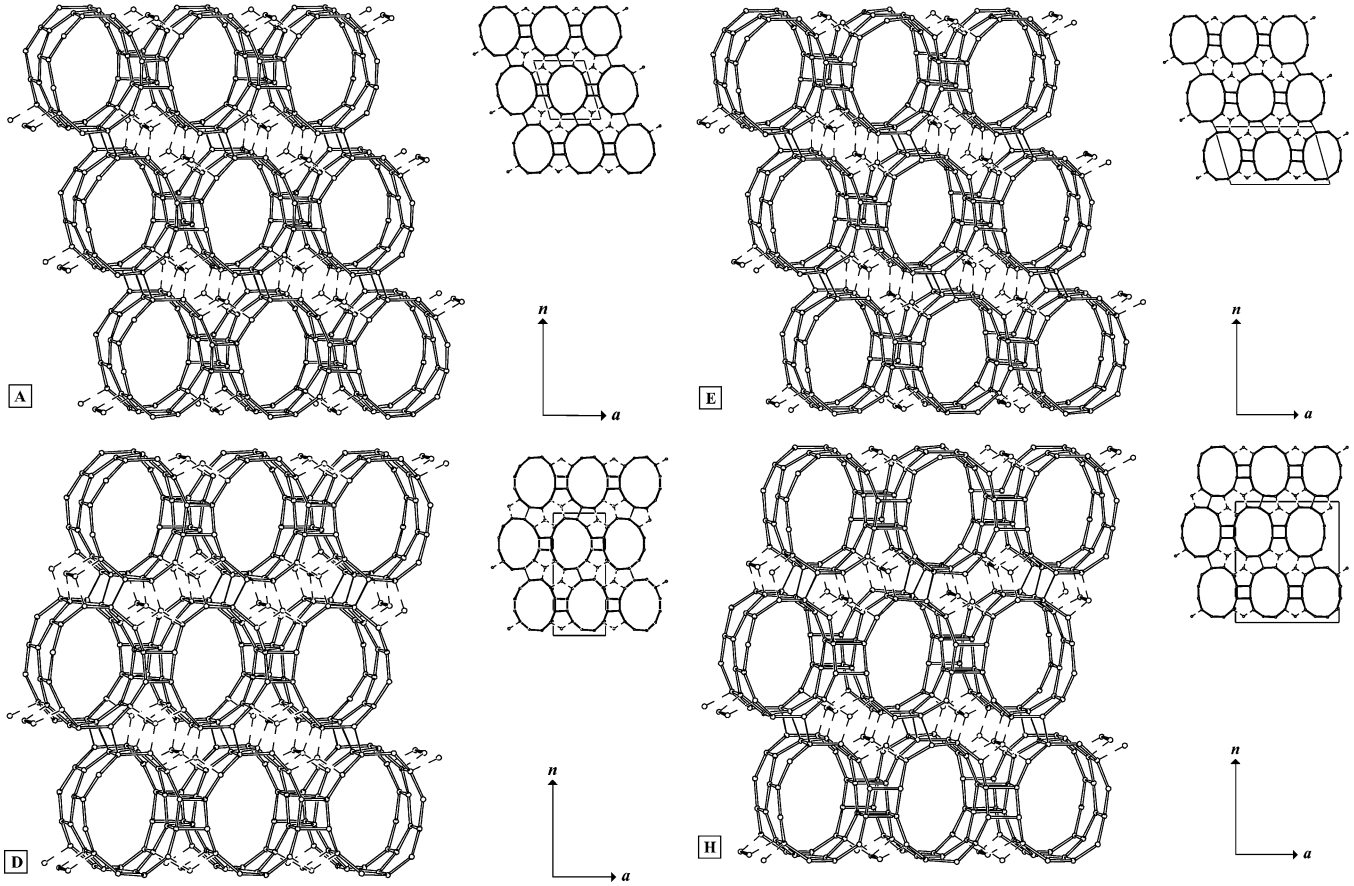

Figure 4. Perspective drawing (left) and parallel projection along the pore axis of the unit cell in standard setting (top right) of the periodic polytypes **A** and **D** in the SSZ-31 family (cf. Table 1). In the simulations (cf. Table 2) the "unit cell" is defined by ***a***, ***b***, and ***n*** (bottom right). The ***a*** axis is in the plane of the PerBU1 and perpendicular to the pore axis, ***b*** is parallel to the pore axis, and ***n*** is parallel to ***a*** × ***b***. Connecting T−T modes between PerBU1s are drawn as single lines and the connections to the space filling T−T dimers (in heavy bold) are striped.

than those that include only PerBU1. This implies that polytypes **E**−**H** need to be included in the description of the disorder in SSZ-31. Intergrowths, which include domains of the polytypes **E**−**H**, will show stacking faults caused by displacements of (100) layers over $^1/_2$***b***. These stacking faults reveal themselves in the ED pattern by diffuse streaks in the *hk*0 projection for $k \neq 2n$ which is in agreement with the observations.

In Figure 7, the XRD pattern calculated with $\alpha = 0.5$, $\beta = 0.25$, and $\gamma = 0.5$ is compared to the experimental XRD pattern. The calculated pattern has been broadened using $w = 0.085$ ($u = 0.1$, $v = -0.18$, and $\gamma = 0.6$). The predicted positions and relative intensities of the sharp and broad peaks are nearly identical to the ones observed in the experimental pattern. The pattern corresponds to the most disordered material where both PerBU1 and PerBU2 occur with equal probability, and the layers are shifted along ***b*** with a 50% probability. Patterns calculated with values of α and γ near 0.5 (± 0.25) do not change dramatically and nearly show the same agreement to experiment as the calculated one shown in Figure 7.

One of the limitations of the model proposed here is that it assumes that the faulted structures of SSZ-31 are built of layers with perfect two-dimensional periodicity (PerBU1 and PerBU2). In the case of ZSM-48, it has been shown that some samples are formed of layers that are not perfectly ordered. Since for SSZ-31 the best agreement between model and experiment is obtained using both PerBU1 and PerBU2 as the building blocks, it is natural to think that there can be layers that are disordered, that is, that are formed of segments of PerBU1 and PerBU2. Although it is possible to approximate the effect of disorder within the layers on the XRD patterns using DIFFaX, the quality of the available experimental data does not warrant the inclusion of yet one more variable in the model. Thus, it remains to be determined, perhaps by detailed electron diffraction studies, if there is disorder within the layers of SSZ-31.

One of the striking features of the model of disorder of SSZ-31 presented here is that although there is no long-range order is these materials, the local structure of the pores in all the models is the same. Since acid catalysis with high-silica zeolites is fundamentally a local phenomenon, differences in catalytic activity and selectivity between different samples of SSZ-31 containing similar Si/Al ratios are thus mainly reflections of the effect of crystal morphology and the distribution of aluminum sites within the crystallites. Since the investigation of the catalytic activity of SSZ-31 is still at an early stage, it is crucial that in the future particle size and shape for all samples is clearly established (by SEM or other techniques), even more so than careful X-ray powder diffraction analyses. This type of characterization will be necessary to establish robust structure−property relationships in this complex class of catalytic materials.

Summary and Conclusions

A new approach to describing the disorder in zeolite SSZ-31 has been presented. The structure is described starting from one-dimensional pores. The pores are formed of rolled-up honeycomb-like sheets of fused T6-rings and the pore aperture contains 12 T atoms. These 1-D units can be arranged into layers to form two kinds of planar building units (PerBU1 and PerBU2). The PerBUs can be stacked to form three-dimensional structures

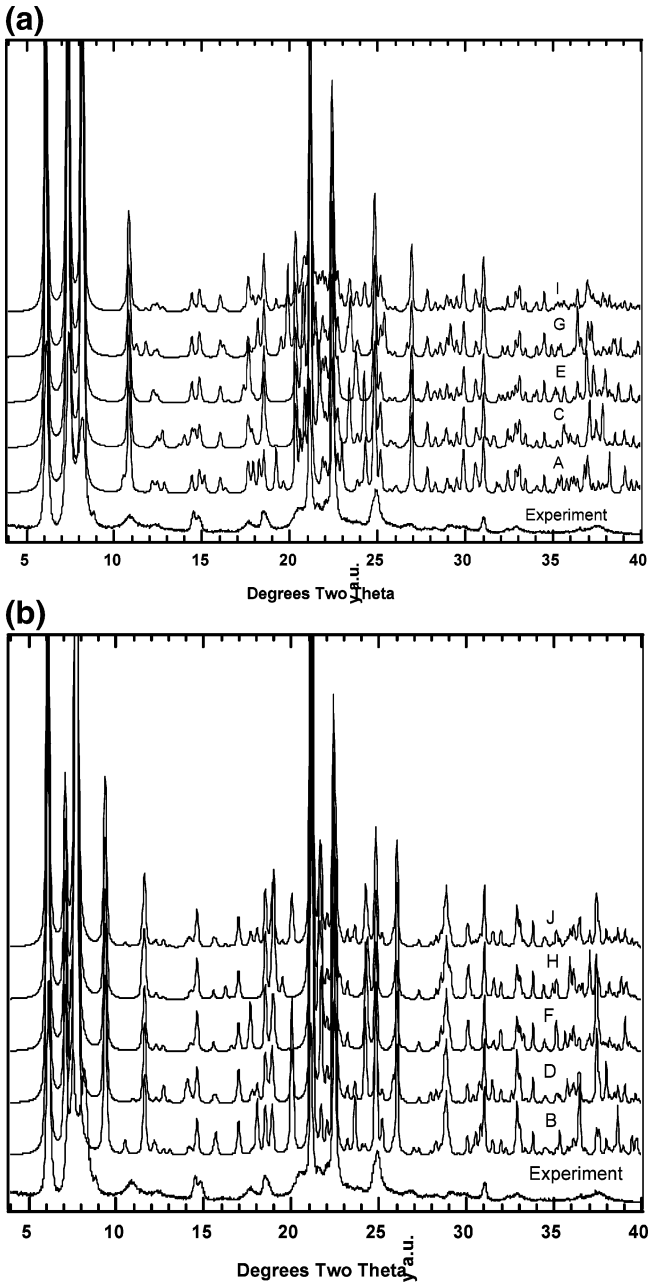

Figure 5. (a) Simulation of XRD patterns of the simplest monoclinic polytypes of SSZ-31 (Cu Kα radiation). Note that all patterns have three peaks at $2\theta = 6.14$, 7.4, and 8.21°, and that these peaks agree with the position of the three peaks of the experimental XRD pattern (bottom). (b) Simulation of XRD patterns of the simplest orthorhombic polytypes of SSZ-31. In this case, the calculated patterns have only two peaks at low 2θ in sharp contrast to the experimental pattern (bottom).

following four connection modes. This approach leads to the discovery of two additional simple polytypes of SSZ-31 (denoted polytypes **I** and **J**) and also shows that it is possible to easily form intergrowths between polytypes **A**−**D** and polytypes **E**−**H**. This last possibility was previously considered very unlikely.[1]

The proposed disorder model is in agreement with the TEM and ED-patterns reported in ref 1. The lateral shifts of the PerBUs of $\pm^1/_6\boldsymbol{a}$ are clearly visible on the TEM image. In the ED pattern these lateral shifts cause diffuse streaks in the *h*0*l* projection for $h \neq 3n$. No diffuse scattering is observed in ED *h*0*l* patterns for $l \neq 3n$. This means that stacking faults, caused by displacements of (100) layers over $\pm^1/_6\boldsymbol{c}$, are very unlikely.

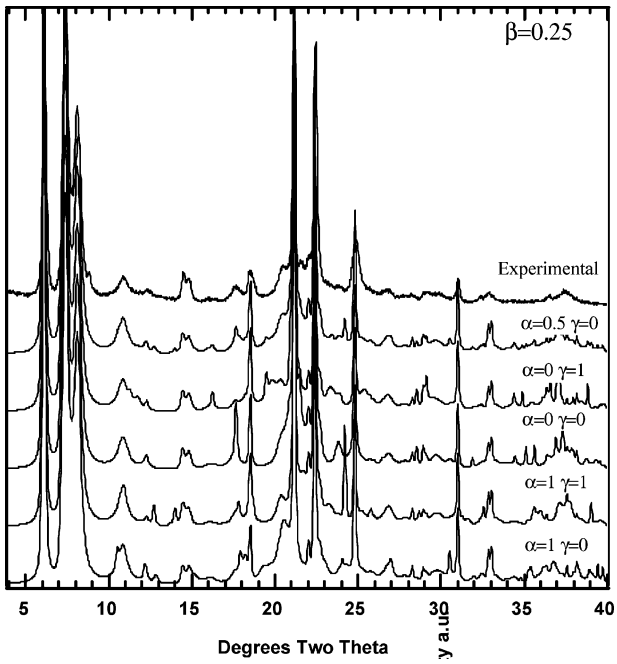

Figure 6. Simulation of XRD patterns of faulted polytypes of SSZ-31 (Cu Kα radiation). In all cases $\beta = 0.25$ and α and γ are either 0 or 1. The top trace is an experimental XRD of SSZ-31. These structures can be thought as faulted forms of the monoclinic polytypes **A** (bottom), **C**, **E**, **G** and **I**.

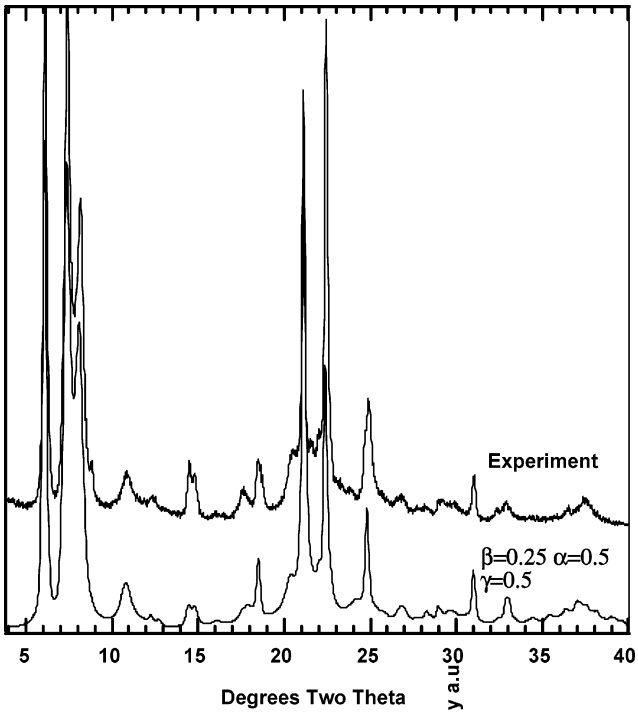

Figure 7. Comparison of experimental XRD pattern of SSZ-31 to a pattern calculated with $\alpha = 0.5$, $\beta = 0.25$, and $\gamma = 0.5$ (Cu Kα radiation). The calculated pattern has been broadened using $w = 0.085$ (and $u = 0.1$, $v = -0.18$, and $\gamma = 0.6$).

Apparently, stacking faults caused by shifts of layers, that break double crankshaft chains and shift the resulting parts perpendicular to the chain axis, are improbable. Stacking faults of the (100) layers, caused by displacements of the layers with respect to each other over $^1/_2\boldsymbol{b}$ along the pore axis, reveal themselves in the ED pattern by diffuse streaks in the *hk*0 projection for $k \neq 2n$. Inclusion in the proposed disorder model of PerBU2 (and thus the polytypes **E**−**H**) is therefore crucial.

TABLE 2: Simplest Ordered Polytypes of SSZ-31 Described Using the Connection Modes and Fault Probabilities

Name	Descriptor[a]	Connection Modes[b]	α	β	γ
		PerBU1			
A	○ ○ ○ ○ ○ ○ ○ ○ ○	($-^1/_6$, 0; $-^1/_6$, 0; $-^1/_6$, 0; …)	1	0	0
B	○ ○ ○ ○ ○ ○ ○ ○ ○	($-^1/_6$, 0; $+^1/_6$, 0; $-^1/_6$, 0; …)	1	1	0
C	○ ○ ○ ● ● ● ○ ○ ○	($-^1/_6$, $^1/_2$; $-^1/_6$, $^1/_2$; $-^1/_6$, $^1/_2$; …)	1	0	1
D	○ ○ ○ ● ● ● ○ ○ ○	($-^1/_6$, $^1/_2$; $+^1/_6$, $^1/_2$; $-^1/_6$, $^1/_2$; …)	1	1	1
		PerBU2			
E	○ ● ○ ○ ● ○ ○ ● ○	($-^1/_6$, 0; $-^1/_6$, 0; $-^1/_6$, 0; …)	0	0	0
F	○ ● ○ ○ ● ○ ○ ● ○	($-^1/_6$, 0; $+^1/_6$, 0; $-^1/_6$, 0; …)	0	1	0
G	○ ● ○ ● ○ ● ○ ● ○	($-^1/_6$, $^1/_2$; $-^1/_6$, $^1/_2$; $-^1/_6$, $^1/_2$; …)	0	0	1
H	○ ● ○ ● ○ ● ○ ● ○	($-^1/_6$, $^1/_2$; $+^1/_6$, $^1/_2$; $-^1/_6$, $^1/_2$; …)	0	1	1
		PerBU1 and PerBU2			
I	○ ○ ○ ○ ● ○ ○ ○ ○	($-^1/_6$, 0; $-^1/_6$, 0; $-^1/_6$, 0; …)	0.5[c]	0	0
J	○ ○ ○ ○ ● ○ ○ ○ ○	($-^1/_6$, 0; $+^1/_6$, 0; $-^1/_6$, 0; …)	0.5[c]	1	0

[a] Empty (○) and filled (●) circles depict pores that are related by translations of $^1/_2 \times 8.4$ Å along the pore direction. [b] The connection modes refer to the displacement along ***a*** and ***b*** between consecutive PerBUs (***a*** = 24.7 Å and ***b*** = 8.4 Å). [c] In these two polytypes, the location of the PerBUs is correlated with an equal amount of each PerBU in the crystal.

In ref 1 it was, in effect, suggested that the only building unit was PerBU1 ($\alpha = 1$) and that the value of γ was different from 0. The present calculations show that better agreement with experiment is obtained when it is assumed that $\beta = 0.25$, that both PerBU1 and PerBU2 are incorporated as building units ($\alpha \approx 0.5$), and that the layers are shifted along ***b*** with a 50% probability ($\gamma \approx 0.5$). This means that the structure of actual samples of SSZ-31 contains nearly the maximum amount of disorder that is possible to obtain within the boundaries of the model proposed here.

The described type of disorder does not block the pores and the local pore topology is the same in all (disordered) models. As a consequence, differences in catalytic behavior of different samples of SSZ-31 are probably due to differences in synthesis conditions (Si/Al ratio), distribution of the Al over the framework positions, and size and morphology of the crystals.

Acknowledgment. We gratefully acknowledge A. Burton from ChevronTexaco Energy Research and Technology Co. (Richmond, California) who provided the sample of SSZ-31. R.F.L. acknowledges P. Kooyman, M.-O. Coppens, and the TU Delft for a visiting position. Funding for this work was partially provided by the National Science Foundation under Grant No. CTS-0085036 to R.F.L.

References and Notes

(1) Lobo, R. F.; Tsapatsis, M.; Freyhardt, C. C.; Chan, I.; Chen, C. Y.; Zones, S. I.; Davis, M. E. *J. Am. Chem. Soc.* **1997**, *119*, 3732−3744.

(2) Bandyopadhyay, R.; Kubota, Y.; Ogawa, M.; Sugimoto, N.; Fukushima, Y.; Sugi, Y. *Chem. Lett.* **2000**, 300−301.

(3) Rao, P.; Ueyama, K.; Kikuchi, E.; Matsukata, M. *Chem. Lett.* **1998**, 311−312.

(4) Ahedi, R. K.; Kubota, Y.; Sugi, Y. *J. Mater. Chem.* **2001**, *11*, 2922−2924.

(5) Camblor, M. A.; Villaescusa, L. A.; Diaz-Cabanas, M. J. *Top. Catal.* **1999**, *9*, 59−76.

(6) Bandyopadhyay, R.; Kubota, Y.; Tawada, S.; Sugi, Y. *Catal. Lett.* **1998**, *50*, 153−158.

(7) Jones, C. W.; Zones, S. I.; Davis, M. E. *Appl. Catal. A−General* **1999**, *181*, 289−303.

(8) Ahedi, R. K.; Tawada, S.; Kubota, Y.; Sugi, Y. *Catal. Lett.* **2001**, *74*, 217−220.

(9) Sugi, Y.; Kubota, Y.; Hanaoka, T.; Matsuzaki, T. *Catal. Surveys Jpn.* **2001**, *5*, 43−56.

(10) Lobo, R. F.; Koningsveld, H. v. *J. Am. Chem. Soc.* **2003**, *124*, 13222−13230.

(11) Treacy, M. M. J.; Newsam, J. M.; Deem, M. W. *Proc. R. Soc. London, Ser. A−Mathematical Physical and Engineering Sciences* **1991**, *433*, 499−520.

(12) Giess, H.; Koningsveld, H. v. Catalog of Disorder in Zeolite Frameworks. http://www.iza-structure.org/databases/ (accessed 2002), last update August 2002.

(13) *Cerius*^{2}, 3.8 edition; Molecular Simulations Inc.: San Diego, CA, 1998.